



**HAL**  
open science

# Seakeeping Behaviour of a Flettner Rotors-Propelled Catamaran in Beam Waves

Fabio Pili, Aurélien Babarit, Félicien Bonnefoy, Grégory Payne

► **To cite this version:**

Fabio Pili, Aurélien Babarit, Félicien Bonnefoy, Grégory Payne. Seakeeping Behaviour of a Flettner Rotors-Propelled Catamaran in Beam Waves. *Journal of Sailing Technology*, 2023, 8 (01), pp.96-117. 10.5957/jst/2023.8.6.96 . hal-04493304

**HAL Id: hal-04493304**

**<https://hal.science/hal-04493304>**

Submitted on 7 Mar 2024

**HAL** is a multi-disciplinary open access archive for the deposit and dissemination of scientific research documents, whether they are published or not. The documents may come from teaching and research institutions in France or abroad, or from public or private research centers.

L'archive ouverte pluridisciplinaire **HAL**, est destinée au dépôt et à la diffusion de documents scientifiques de niveau recherche, publiés ou non, émanant des établissements d'enseignement et de recherche français ou étrangers, des laboratoires publics ou privés.

# Seakeeping behaviour of a Flettner rotors-propelled catamaran in beam waves

## Fabio Pili

Nantes Université, École Centrale Nantes, CNRS, LHEEA, UMR 6598, F-44000 Nantes, France.  
fabio.pili@ec-nantes.fr.

## Aurélien Babarit

Nantes Université, École Centrale Nantes, CNRS, LHEEA, UMR 6598, F-44000 Nantes, France.

## Félicien Bonnefoy

Nantes Université, École Centrale Nantes, CNRS, LHEEA, UMR 6598, F-44000 Nantes, France.

## Grégory S. Payne

Farwind Energy, 44300 Nantes, France.

**Abstract.** This paper deals with the seakeeping of a catamaran propelled by Flettner rotors. The case study is an energy ship. The prediction of the roll motion of such a ship is of particular interest since she will mostly sail in beam seas. We used a numerical model based on the boundary element method (BEM) to deal with the interactions of the ship with waves. It is supplemented by a model for the aerodynamic damping effect due to the rotors, the gyroscopic effects from the rotors and by the ITTC correction for roll damping. In the present study, it has been assumed that the Flettner rotors can be modelled as a distribution of elementary airfoils whose lift and drag depend on the local apparent wind speed. Interaction effects between the rotors and between the hull and rotors have been neglected. Regular waves have been investigated. For the considered case study, it is found that the Flettner rotors can have a small destabilizing effect or a small stabilizing effect on the ship motion depending on the ship speed and the rotors' rotational speed.

**Keywords:** Flettner rotor; Seakeeping; Roll Motion; Sail aerodynamics; Boundary Element Method; Energy ship

## 1 INTRODUCTION

Climate change is a significant threat to our societies. To prevent disastrous outcomes, the increase in global temperature must be kept below 2°C according to IPCC et al. (2018). It requires a drastic reduction in global greenhouse gas emissions, a goal which requires the development of new technologies including wind assisted ship propulsion (WASP) systems (soft sails, wingsails, Flettner rotors, kite, turbosails) and marine renewable energy (MRE) converters (offshore wind turbines, wave energy converters, tidal energy converters).

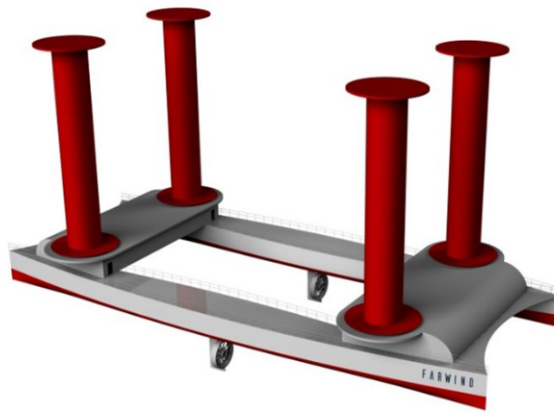
In this context, the company Farwind Energy was founded in 2020 in order to develop new systems for offshore wind energy harvesting ([www.farwind-energy.com](http://www.farwind-energy.com)). Those systems are based on the energy ship technology (Salomon, 1982). An energy ship is a vessel propelled by the wind and equipped with hydroturbines so that electrical power is produced while sailing. The generated electricity is stored on board, either in batteries or through its conversion into fuel (hydrogen, ammonia, methanol, etc.). A key advantage of the energy ship is that it enables the harvesting of far offshore wind energy which, despite being the second greatest renewable energy source on the planet, is left largely unexploited to date. Examples of proposed energy ship concepts are described in Kim and Park (2010), Platzer et al. (2014), Ouchi and Henzie (2017), Gilloteaux and Babarit (2017).

Figure 1 shows a picture of an example energy ship design which has been proposed by Ecole Cen-

trale de Nantes (Babarit et al., 2021). It consists of a catamaran vessel propelled by four Flettner rotors. It is equipped with two hydroturbines attached underneath the hull. Further details on this design are provided in Table 1.

**Table 1. Energy ship design specifications**

Hull	Unit	Value
Length	m	80
Breadth	m	31.7
Draft	m	2.1
Displacement	t	1035
$X_G$	m	0.000
$Y_G$	m	0.003
$Z_G$	m	7.430
Wind propulsion	Unit	Value
Type	-	Flettner rotors
Number	-	4
Rotor height	m	35
Rotor diameter	m	5
Rotor mass	t	79
Rotor drive power (max)	kW	143



**Figure 1. Artist's view of the energy ship design**

According to Babarit et al. (2021), maximum power production is achieved when the ship is sailing beam wind. In practice, beam wind will very often correspond to beam sea conditions (as waves are generated by the wind). Therefore, it is critical to investigate in the early design phases whether wave-induced roll motion may be a challenge regarding the ship's safety and operability.

Several studies have been published in the scientific literature regarding the roll motion prediction of seagoing vessels. The fundamental equation of motion of ships and offshore structures in waves can be found in e.g. Faltinsen (1993). Ikeda (1978) conducted several studies to investigate the roll damping components of marine vessels. The outcome of his works was a set of empirical formulas for various roll damping components for mono-hulls and catamaran vessels, which are still recommended by ITTC (2011). Katayama et al. (2011) carried out experimental investigations on the roll damping characteristics of multi-hulls vessels, both with and without forward speed. They showed that the effect of forward speed on roll damping is significant for a catamaran, especially for low values of forced roll amplitudes at low Froude numbers ( $F_n < 0.3$ ).

It is well known to yachtsmen that the roll of a yacht with its sails up is significantly smaller than that

without sail. The same effect has been reported for wind-assisted ships (Kuuskoski and V., 2023). Aerodynamic damping effects of wind propulsion devices including Flettner rotors were examined theoretically by F.M.Sinclair (1991). That work showed that if Flettner rotors operate at a sufficiently high spin ratio (greater than 4), they have a stabilizing effect on roll motion. However, it was also observed that they can be destabilizing for apparent wind angles between  $40^\circ$  and  $60^\circ$  and spin ratio equal to 2. No data is available for other values of spin ratio. Copuroglu and Pesman (2018) investigated the effect of Flettner rotors on roll motion of a cargo ship using CFD (Lattice Boltzmann methods). It was found that the maximum roll angle was increased. However, results show that the increase is essentially due to the non-zero heel angle associated with the presence of the rotors. The effect of the rotors on the roll motion amplitude appears to be much smaller.

Vertical spinning cylinders, such as Flettner rotors, induce a gyroscopic effect which may affect the dynamic stability of a ship. Gyrostabilizer devices (Demir (2020)) utilizing this effect have been developed in order to reduce the motion of leisure vessels. Perez and Steinmann (2009) investigated the roll damping characteristics of a gyro stabilizer control system using a numerical model combining the vessel and a gyrostabilizer. They proposed improved methodologies for gyrostabilizer control design in which the controller forces the gyrostabilizer to behave like an additional roll damping source using only information about the precession motion. To the authors' knowledge, an analysis of the gyroscopic effect of Flettner rotors on the motion of ships has not yet been published in the scientific literature. This may be because this effect is expected to be small (because of the relatively slow rotational velocities of the rotors and of their comparatively small dimension inducing a comparatively small inertia of the rotating parts). However, in the case of the energy ship considered in this study, the Flettner rotors have great dimensions. Therefore it is important to evaluate the influence of gyroscopic effect on the seakeeping of energy ships.

Thus, in this study, we investigate the effect of Flettner rotors on the roll motion of an energy ship. Section 2.1 presents the rotor model in terms of aerodynamic forces and gyroscopic loads. Section 2.2 describes the seakeeping model of the ship including various damping sources. Section 3.1 addresses the accuracy of the rotor model. Section 3.2 shows the results of seakeeping simulations with active flettner rotors for the energy ship design shown in Figure 1. Section 3.3 presents the gyroscopic effect of the Flettner rotors on the seakeeping behaviour for the energy ship considered. Finally, the effect of varying the rotors' mass is discussed in section 3.4.

## 2 MODEL

To predict the motions of the ship in the six degrees of freedom (DoF), let us define two coordinate systems (Figure 2):

- The Earth-fixed reference frame  $(O, \vec{x}_0, \vec{y}_0, \vec{z}_0)$  where  $z = 0$  is the water surface at rest. This reference frame is oriented upwards.
- The Ship-fixed reference frame  $(G, \vec{x}_b, \vec{y}_b, \vec{z}_b)$  where  $G$  is the boat's center of gravity,  $\vec{x}_b$  is positive forward,  $\vec{z}_b$  positive upwards and aligned with the rotor axis,  $\vec{y}_b$  is oriented such that the reference frame is right-handed. Let  $\varphi$  be the roll angle,  $\theta$  be the pitch angle and  $\psi$  be the yaw angle.

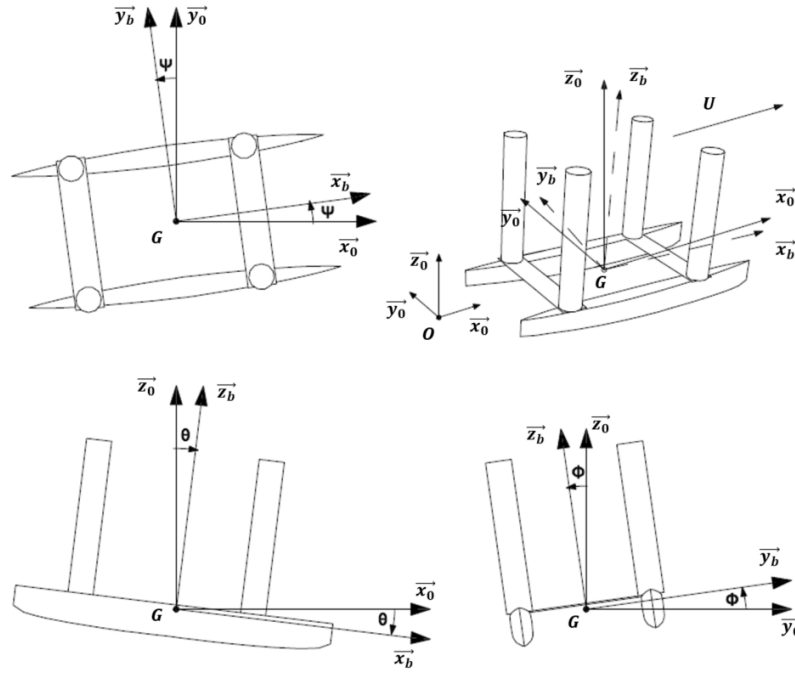


Figure 2. Seakeeping coordinate systems

## 2.1 Flettner rotor model

### 2.1.1 Aerodynamic force and aerodynamic damping matrix in quasi-static approach

In this study, the Flettner rotors are modelled as a distribution of elementary airfoils whose lift and drag depend on the local apparent wind speed. The aerodynamic interactions between the rotors have been neglected. The diameter and height of the rotor are denoted  $D$  and  $H$  respectively. The aerodynamic force  $\mathbf{F}_a$  acting on a Flettner rotor can then be written:

$$\mathbf{F}_a = \int_{h=0}^H \frac{1}{2} \rho_a D V(h)^2 \begin{pmatrix} C_x(h) \\ C_y(h) \\ 0 \end{pmatrix}_b dh \quad (1)$$

where  $\rho_a$  is the air density,  $V(h)$  is the apparent wind speed projected in the plane perpendicular to the rotor axis and passing by the point located at the distance  $h$  from the rotor bottom along the rotor axis (center of strip  $\mathbf{P}(h)$  of the rotor),  $C_x$  is the thrust coefficient,  $C_y$  is the side force coefficient.

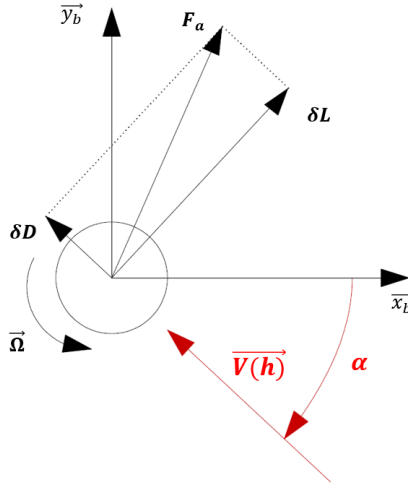


**Figure 3. Flettner rotor force diagram**

The local lift force  $\delta L$ , local drag force  $\delta D$ , thrust and side force coefficients are related to the local lift coefficient  $C_L$  and drag  $C_D$  coefficient (Figure 3):

$$\begin{aligned}
 C_x &= C_L \sin(\alpha) - C_D \cos(\alpha) \\
 C_y &= C_L \cos(\alpha) + C_D \sin(\alpha) \\
 \delta \mathbf{L}(h) &= \frac{1}{2} \rho_a C_L D V(h)^2 dh \\
 \delta \mathbf{D}(h) &= \frac{1}{2} \rho_a C_D D V(h)^2 dh
 \end{aligned} \tag{2}$$

where  $\alpha$  is the local apparent wind angle.

The apparent wind speed depends on the true wind speed and on the ship motion. Let  $W(z)$  be the true wind speed and  $\beta$  the true wind angle. Let  $(\chi_B, \xi_B, \zeta_B)$  be the coordinates of the rotor bottom in the ship reference frame. Assuming that the ship rotations are small, one can show that the ship-induced velocity of point  $\mathbf{P}$  along the rotor axis can be written:

$$\mathbf{U}(\mathbf{P}) = \begin{pmatrix} \dot{X} + (\zeta_B + h)\dot{\theta} - \xi_B \dot{\psi} \\ \dot{Y} + \chi_B \dot{\psi} - (\zeta_B + h)\dot{\varphi} \\ \dot{Z} + \xi_B \dot{\varphi} - \chi_B \dot{\theta} \end{pmatrix}_b \tag{3}$$

Therefore, the total apparent wind speed  $\mathbf{V}_T$  is:

$$\begin{aligned}
 \mathbf{V}_T(\mathbf{P}) &= \mathbf{W}(\mathbf{P}) - \mathbf{U}(\mathbf{P}) \\
 \mathbf{V}_T(\mathbf{P}) &= \begin{pmatrix} -W(z) \cos(\beta + \psi) - \dot{X} - (\zeta_B + h)\dot{\theta} + \xi_B \dot{\psi} \\ W(z) \sin(\beta + \psi) - \dot{Y} - \chi_B \dot{\psi} + (\zeta_B + h)\dot{\varphi} \\ W(z) \theta \cos(\beta + \psi) + W(z) \varphi \sin(\beta + \psi) - \dot{Z} - \xi_B \dot{\varphi} + \chi_B \dot{\theta} \end{pmatrix}_b
 \end{aligned} \tag{4}$$

The apparent wind speed projected in the plane perpendicular to the rotor  $V(h)$  and the apparent wind angle  $\alpha$  are thus given by:

$$\begin{cases} V(h)^2 = & \left( \begin{aligned} & (-W(z) \cos(\beta + \psi) - \dot{X} - (\zeta_B + h)\dot{\theta} + \xi_B \dot{\psi})^2 + \\ & (W(z) \sin(\beta + \psi) - \dot{Y} - \chi_B \dot{\psi} + (\zeta_B + h)\dot{\varphi})^2 \end{aligned} \right) \\ V(h) \cos \alpha = & W(z) \cos(\beta + \psi) + \dot{X} + (\zeta_B + h)\dot{\theta} - \xi_B \dot{\psi} \\ V(h) \sin \alpha = & W(z) \sin(\beta + \psi) - \dot{Y} - \chi_B \dot{\psi} + (\zeta_B + h)\dot{\varphi} \end{cases} \tag{5}$$

In Equation 4, the true wind speed depends on the vertical coordinate  $z = Z - \chi_B \theta + \xi_B \varphi + \zeta_B + h$  to take into account the atmospheric boundary layer. This dependency can be modelled by:

$$W(\mathbf{z}) = W_r \left( \frac{z}{z_r} \right)^\sigma \quad (6)$$

where  $z_r$  is the reference height (usually 10 m) and  $\sigma$  is the Hellmann coefficient. According to Touma (1977)  $\sigma = 0.11$  can be used for open water.

Let  $\omega$  be the rotor's rotational speed. Let  $SR(h) = \omega D / (2V(h))$  be the local spin ratio at height  $h$  along the rotor axis. According to Tillig and Ringsberg (2020), the lift and drag coefficients of the rotor  $C_L$  and  $C_D$  can be expressed as function of the spin ratio as:

$$\begin{aligned} C_L &= 0.0046SR^5 + 0.11SR^4 - 0.98SR^3 + 3.1SR^2 - 0.10SR \\ C_D &= -0.0017SR^5 + 0.046SR^4 - 0.44SR^3 + 1.7SR^2 - 1.6SR + 0.64 \end{aligned} \quad (7)$$

Note that the lift and drag coefficients in Equation 7 are 2D coefficients that have been derived from CFD results of Li and Leer-Andersen (2012) and have been corrected to better match the full-scale measurements (see Tillig and Ringsberg, 2020). Those coefficients were applied to each strip of the rotors. The moment  $\mathbf{M}_a$  at the bottom of the rotor  $\mathbf{B}$  is:

$$\mathbf{M}_a(\mathbf{B}) = \int_{h=0}^H \frac{1}{2} \rho_a D V^2(h) \begin{pmatrix} -hC_y(h) \\ hC_x(h) \\ 0 \end{pmatrix}_b dh \quad (8)$$

Finally, let us define the aerodynamic damping matrix  $\mathbf{B}_a$  by:

$$B_{a,ij} = \frac{\partial \tilde{F}_{a,i}}{\partial \dot{X}_j} \quad (9)$$

where  $\tilde{\mathbf{F}}_a = [\mathbf{F}_a, \mathbf{M}_a(\mathbf{G})]^T$  is the generalized aerodynamic force and  $\mathbf{X} = [X, Y, Z, \varphi, \theta, \psi]^T$  is the ship motion. All the previous equations define what we consider the quasi-static model of the Flettner rotors for the example energy ship design shown in Figure 1.

### 2.1.2 Case of pure roll motion and linearization

In principle, the stabilizing effect of the rotor could be analyzed by assessing the eigenvalues of the aerodynamic damping matrix  $\mathbf{B}_a$ . However, its expression is too complex in the general case to perform such a task by hand. Moreover, in this study, the focus is on the effect of the rotors on roll motion. Therefore, in this section, let us assume that the ship is moving forward with constant speed ( $\dot{X} = U$ ) and that it is moving only in roll ( $\dot{Y} = \dot{Z} = 0$  and  $\dot{\theta} = \dot{\psi} = 0$ ). The dependence of the true wind speed on the height is also neglected ( $W(z) = W_{10}$ ) and the ship is supposed to sail beam wind ( $\beta = 90^\circ$ ).

Recalling that the roll motion is supposed to be small, the apparent wind speed Equation 5 simplifies to:

$$\begin{cases} V(h) &= V_0 \left( 1 + \frac{W_{10}}{V_0^2} (\zeta_B + h) \dot{\varphi} \right) \\ V(h) \cos \alpha &= U \\ V(h) \sin \alpha &= W_{10} + (\zeta_B + h) \dot{\varphi} \end{cases} \quad (10)$$

where  $V_0^2 = W_{10}^2 + U^2$ .

Let us recall that the aerodynamic moment along the x-axis of the ship at the bottom of the rotor is:

$$M_{a,x}(\mathbf{B}) = - \int_{h=0}^H \frac{1}{2} \rho_a D V(z)^2 h C_y dh \quad (11)$$

It can be rewritten:

$$M_{a,x}(\mathbf{B}) = - \int_{h=0}^H \frac{1}{2} \rho_a D h V(z) V(z) C_y dh \quad (12)$$

According to equations 2 and 10:

$$\begin{aligned} V(h)C_y(h) &= C_L(h)V(h) \cos(\alpha) + C_D(h)V(h) \sin(\alpha) \\ V(h)C_y(h) &= C_L(h)U + C_D(h)(W_{10} + (\zeta_B + h)\dot{\varphi}) \\ V(h)C_y(h) &= V_0 C_y(0) + \left( U \frac{\partial C_L}{\partial \dot{\varphi}} \Big|_{\dot{\varphi}=0} + (\zeta_B + h)C_D(0) \right) \dot{\varphi} + o(\dot{\varphi}) \end{aligned} \quad (13)$$

where the lift and drag coefficients have been replaced by their Taylor expansion at first order.

Using Equation 13 and Equation 10, one can show that the aerodynamic moment in roll can be written:

$$\begin{aligned} M_{a,x}(\mathbf{B}) &= M_{a,x,0}(\mathbf{B}) \\ &- \frac{1}{2} \rho_a D V_0 H^2 \left\{ \frac{U}{H^2} \int_{h=0}^H h \frac{\partial C_L}{\partial \dot{\varphi}} \Big|_{\dot{\varphi}=0} dh + \left( \frac{1}{2} \zeta_B + \frac{H}{3} \right) (C_{D,i,0} + \frac{W_{10}}{V_0} C_{y,i,0}) \right\} \dot{\varphi} + o(\dot{\varphi}) \end{aligned} \quad (14)$$

By inspecting Equation 14, one can see that the aerodynamic moment induced by roll is stabilizing if:

$$\int_{h=0}^H h \frac{\partial C_L}{\partial \dot{\varphi}} \Big|_{\dot{\varphi}=0} dh > - \frac{H^2}{U} \left( \frac{1}{2} \zeta_B + \frac{H}{3} \right) (C_{D,i,0} + \frac{W_{10}}{V_0} C_{y,i,0}) \quad (15)$$

Thus, let us consider the derivative of the lift coefficient with respect to  $\dot{\varphi}$ . One can write:

$$\frac{\partial C_L}{\partial \dot{\varphi}} = \frac{\partial C_L}{\partial SR} \frac{\partial SR}{\partial V} \frac{\partial V}{\partial \dot{\varphi}} \quad (16)$$

According to equations 7 and 10 and to the definition of the spin ratio:

$$\begin{aligned} \frac{\partial C_L}{\partial SR} &= 0.023SR^4 + 0.46SR^3 - 2.9SR^2 + 6.3SR - 0.10 \\ \frac{\partial SR}{\partial V} &= - \frac{\omega D}{2V^2} = - \frac{SR}{V} \\ \frac{\partial V}{\partial \dot{\varphi}} &= \frac{W_{10}}{V_0} (\zeta_B + h) \end{aligned} \quad (17)$$

Thus, by combining equations 17 and Equation 15, one can show:

$$\begin{aligned} \int_{h=0}^H h \frac{\partial C_L}{\partial \dot{\varphi}} \Big|_{\dot{\varphi}=0} dh &= \\ &- (0.023SR_0^4 + 0.46SR_0^3 - 2.9SR_0^2 + 6.3SR_0 - 0.10) \frac{SR_0}{V_0} \frac{W_{10}}{V_0} \left( \zeta_B \frac{H^2}{2} + \frac{H^3}{3} \right) \end{aligned} \quad (18)$$

Taking this relation into account, the stabilization condition 15 can be re-written:

$$\underbrace{\frac{V_0^2}{UW_{10}}(C_{D,i,0} + \frac{W_{10}}{V_0}C_{y,i,0}) - 0.023SR_0^5 - 0.46SR_0^4 + 2.9SR_0^3 - 6.3SR_0^2 + 0.10SR_0}_{\lambda_{Tillig}} > 0 \quad (19)$$

In practice, the typical range of spin ratio of Flettner rotors is  $SR \in [0, 5]$ . Typical true wind velocity and ship velocity may be  $W_{10} = 9$  m/s and  $U = [6, 9, 12]$  m/s respectively. Figure 4 shows the stabilization condition as a function of the spin ratio for these velocities. For  $U = 9$  m/s, one can see that if  $SR \in [0, \simeq 0.5] \cup [\simeq 1.5, \simeq 3.1]$  the Flettner rotor effect is stabilizing. However, if  $SR \in [\simeq 0.5, \simeq 1.5]$  or if  $SR > 3.1$ , it is found to be destabilizing. Moreover, for  $SR > 3.1$ , the destabilizing effect increases with increasing spin ratio. Figure 4 also shows that the destabilizing effect can be mitigated by reducing ship speed, although to a limited extent.

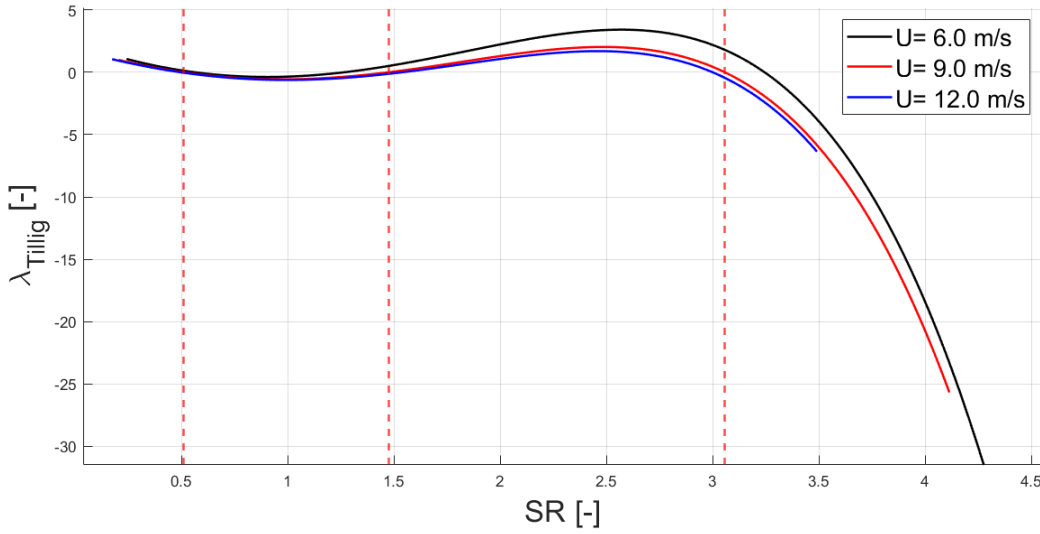


**Figure 4. Stability condition for a single Flettner rotor in pure roll with  $W_{10} = 9$  m/s using lift and drag coefficients of Tillig and Ringsberg (2020)**

Our results disagree with those of F.M.Sinclair (1991). Indeed, according to her simulations, the effect is destabilizing for  $SR = 2$  and stabilizing for  $SR = 4$ . The difference can be attributed to the used lift and drag coefficients. Indeed, F.M.Sinclair (1991) used aerodynamic coefficients which were obtained through experiments (Clayton, 1985) carried out at a Reynolds number  $Re \approx 10^5$  whereas those used in the present study were derived from sea trials, corresponding to  $Re > 10^6$ . Using the lift and drag coefficients used in F.M.Sinclair (1991), the stability condition becomes:

$$\underbrace{\frac{V_0^2}{UW_{10}}(C_{D,i,0} + \frac{W_{10}}{V_0}C_{y,i,0}) - 3.9SR_0}_{\lambda_{Sinclair}} > 0 \quad (20)$$

Figure 5 shows this stability condition as a function of the spin ratio and ship forward speed  $U$ . In this case the results better agree with hers: i.e destabilizing effect at low SRs and stabilizing effect at high SRs. The critical spin ratio for which the stability condition changes from a destabilizing effect to a stabilizing effect is  $SR = 2.2$  for  $U = 9$  m/s (it is between  $SR=2$  and  $SR=4$  in F.M.Sinclair (1991)). Overall, those results show that the stabilizing or destabilizing effect is highly dependent on the aerodynamic coefficients.

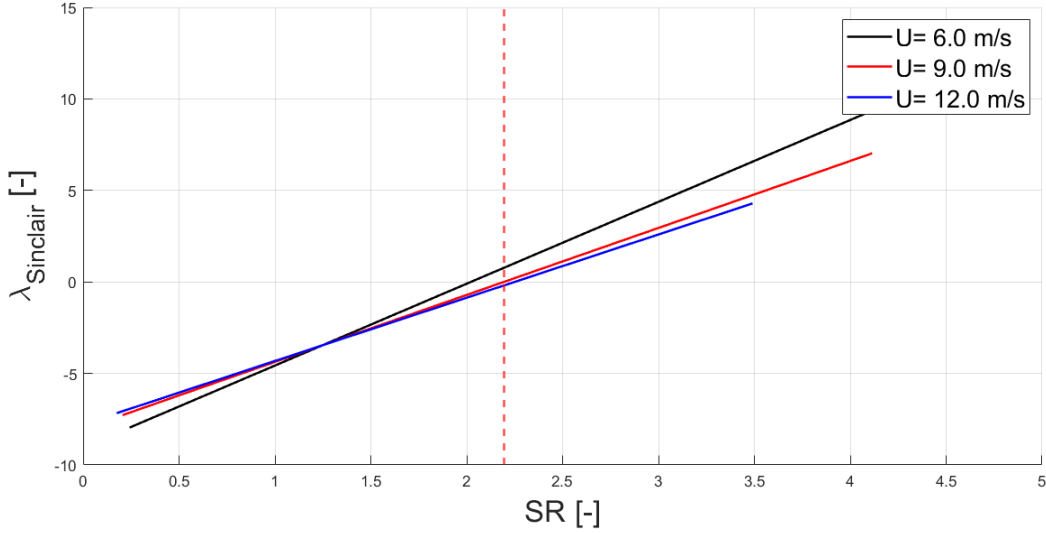


**Figure 5. Stability condition for a single Flettner rotor in pure roll with  $W_{10} = 9$  m/s using lift and drag coefficients of F.M.Sinclair (1991).**

### 2.1.3 Gyroscopic loads from rotors

The gyroscopic effect is a phenomenon observed with rotating objects when external forces are applied to them. It causes a change in the orientation of the rotation axis (precession). This effect comes from the conservation of angular momentum. Conversely, applying a motion to a rotating object generates a force which is the gyroscopic force.

Let us express the equation of motion of a rotor  $k$  rigidly mounted on a ship. The rotational velocity of that rotor is denoted  $\omega_k$ . Let  $m_R$  be the mass of the rotor and  $\gamma(\mathbf{G}_{Rk})$  be the acceleration of the rotor's center of gravity  $\mathbf{G}_{Rk}$ . Let  $\sigma(\mathbf{G}_{Rk})$  be its angular momentum and  $\delta(\mathbf{G}_{Rk})$  be its dynamic moment expressed at its center of gravity. The equation of motion of a single  $k$  rotor in the ship-fixed reference frame is:

$$\begin{cases} m_R \gamma(\mathbf{G}_{R,k})|_b = \mathbf{F}_{a,k}|_b + \mathbf{F}_{g,k}|_b + \mathbf{F}_{j,k}|_b \\ \delta(\mathbf{G}_{Rk})|_b = \mathbf{M}_{a,k}|_b + \mathbf{M}_{g,k}|_b + \mathbf{M}_{j,k}|_b \end{cases} \quad (21)$$

where  $\mathbf{F}_{a,k}|_b$  and  $\mathbf{M}_{a,k}|_b$  are the aerodynamic force and moment (see section 2.1.1),  $\mathbf{F}_{g,k}|_b$  and  $\mathbf{M}_{g,k}|_b$  are the gravity force and moment, and  $\mathbf{F}_{j,k}|_b$  and  $\mathbf{M}_{j,k}|_b$  are the forces and moments in the joint connecting the rotor to the ship.

Let us further assume that the ship dynamic motions are small, i.e:

$$\begin{cases} X(t) = Ut + \tilde{X}(t) \text{ where } U \text{ is constant and } \tilde{X} \ll 1 \\ Y(t) = U_{\perp}t + \tilde{Y}(t) \text{ where } U_{\perp} \text{ is constant and } \tilde{Y} \ll 1 \\ Z(t) \ll 1 \\ \varphi(t) \ll 1 \\ \theta(t) \ll 1 \\ \psi(t) \ll 1 \end{cases} \quad (22)$$

Note that  $U$  corresponds to the ship forward speed and  $U_{\perp}$  corresponds to the drift velocity.

Using those assumptions, the rotor's angular velocity vector  $\Omega_k$  can be written in the ship-fixed frame:

$$\Omega_k|_b = \begin{pmatrix} \dot{\varphi} \\ \dot{\theta} \\ \dot{\psi} + \omega_k \end{pmatrix} \quad (23)$$

Let  $\mathbf{II}_k$  be the rotor's inertial matrix. Its angular momentum  $\sigma(\mathbf{G}_{Rk})$  expressed at the rotor's centre of gravity in the ship-fixed reference frame is:

$$\sigma(\mathbf{G}_{Rk})|_b = \mathbf{II}_k \Omega_k|_b \quad (24)$$

Let  $(\chi_{r,k}, \xi_{r,k}, \zeta_{r,k})$  be the coordinates of the rotor's centre of gravity in the ship-fixed reference frame. Taking into account the small amplitude motions assumption, one can show that the rotor's acceleration vector  $\gamma(\mathbf{G}_{r,k})$  can be written:

$$\gamma(\mathbf{G}_{r,k})|_b = \begin{pmatrix} \ddot{X} \\ \ddot{Y} \\ \ddot{Z} \end{pmatrix} + \begin{pmatrix} 0 \\ 0 \\ U\dot{\theta} - U_{\perp}\dot{\varphi} \end{pmatrix} + \mathbf{T}_{r,k} \begin{pmatrix} \ddot{\varphi} \\ \ddot{\theta} \\ \ddot{\psi} \end{pmatrix} \quad (25)$$

$$\text{with } \mathbf{T}_{r,k} = \begin{pmatrix} 0 & (\zeta_{r,k} + h) & -\xi_{r,k} \\ -(\zeta_{r,k} + h) & 0 & \chi_{r,k} \\ \xi_{r,k} & -\chi_{r,k} & 0 \end{pmatrix}$$

Equation 25 can be rewritten:

$$\gamma(\mathbf{G}_{Rk})|_b = \begin{pmatrix} \mathbf{I}_{3 \times 3} & \mathbf{T}_{r,k} \end{pmatrix} \ddot{\mathbf{X}} + \begin{pmatrix} 0 \\ 0 \\ U\dot{\theta} - U_{\perp}\dot{\varphi} \end{pmatrix} \quad (26)$$

As for the rotor's dynamic moment, one can show that it can be written at the boat centre of gravity in the ship-fixed reference frame:

$$\delta_{r,k}(\mathbf{G})|_b = \delta \mathbf{m}_{r,k} \ddot{\mathbf{X}} + \begin{pmatrix} 0 \\ 0 \\ II_{k,zz} \dot{\omega}_k \end{pmatrix} + \mathbf{b}_{j,k} \begin{pmatrix} \dot{\varphi} \\ \dot{\theta} \\ \dot{\psi} \end{pmatrix} \quad (27)$$

With:

$$\delta \mathbf{m}_{r,k} = \begin{bmatrix} m_k \mathbf{T}_{r,k} & \mathbf{II}_k + m_k \mathbf{T}_{r,k}^2 \end{bmatrix} \quad (28)$$

$$\mathbf{b}_{j,k} = \begin{pmatrix} m_k U_{\perp} (\zeta_{r,k} + h) & II_{k,zz} \omega_k - m_k U (\zeta_{r,k} + h) & 0 \\ -II_{k,zz} \omega_k + m_k U_{\perp} \chi_{r,k} & -m_k U \chi_{r,k} & 0 \\ 0 & 0 & 0 \end{pmatrix} \quad (29)$$

The last term in Equation 27 corresponds to the gyroscopic effects.

## 2.2 Seakeeping model

The seakeeping model is based on the classical equation of motion of a ship in regular waves augmented with the hull and appendages resistance  $\tilde{\mathbf{R}}_w(\mathbf{G})|_b$ , the effect of the rotors on the hull  $\sum_{k=1}^N \tilde{\mathbf{F}}_{j,k}(\mathbf{G})|_b$ , and an additional buoyancy force  $\tilde{\mathbf{F}}_b(\mathbf{G})|_b$  which is required to compensate the mass of the rotors:

$$[\mathbf{M} + \mathbf{A}(\omega_e)] \ddot{\mathbf{X}} + \mathbf{B}(\omega_e) \dot{\mathbf{X}} + \mathbf{K} \mathbf{X} = A_s(\omega_e) \mathbf{F}_e(\omega_e) + \tilde{\mathbf{R}}_w(\mathbf{G})|_b - \sum_{k=1}^N \tilde{\mathbf{F}}_{j,k}(\mathbf{G})|_b + \tilde{\mathbf{F}}_b(\mathbf{G})|_b \quad (30)$$

where we recall that  $\mathbf{X}$  is the ship motion,  $\mathbf{M}$  is the generalized mass matrix of the ship,  $\mathbf{A}(\omega_e)$  is the added mass matrix,  $\mathbf{B}(\omega_e)$  is the wave radiation damping matrix,  $\mathbf{K}$  is the hydrostatic stiffness matrix,  $\mathbf{F}_e(\omega_e)$  is the wave excitation force transfer function,  $A_s$  is the wave amplitude and  $\omega_e$  is the encounter frequency.

The hull and appendages resistance  $\tilde{\mathbf{R}}_w(\mathbf{G})|_b$  is modelled as:

$$\tilde{\mathbf{R}}_w(\mathbf{G})|_b = \tilde{\mathbf{R}}_{w,0}(\mathbf{G})|_b - \mathbf{B}_{\text{ITTC}}(\omega_e)\dot{\mathbf{X}} \quad (31)$$

where  $\tilde{\mathbf{R}}_{w,0}(\mathbf{G})|_b$  is the hull and appendages resistance in steady state and  $\mathbf{B}_{\text{ITTC}}$  is the empirical damping matrix correction suggested by ITTC (2011).

It is assumed that the center of effort (buoyancy) of the additional buoyancy force is close to the ship gravity center. Thus, one can show:

$$\tilde{\mathbf{F}}_b(\mathbf{G})|_b = \sum_{k=1}^N m_k g \begin{pmatrix} -\theta \\ \varphi \\ 1 \\ 0 \\ 0 \\ 0 \end{pmatrix} \quad (32)$$

According to equations 21, 26 and 27, and assuming that the rotational velocities of the rotor are constant ( $\dot{\omega}_k = 0$ ), the effect of the rotors on the hull can be written:

$$\sum_{k=1}^N \tilde{\mathbf{F}}_{j,k}(\mathbf{G})|_b = \left[ \sum_{k=1}^N \delta \mathbf{m}_{r,k} \right] \ddot{\mathbf{X}} + \left[ \sum_{k=1}^N \mathbf{B}_{j,k} \right] \dot{\mathbf{X}} - \sum_{k=1}^N \tilde{\mathbf{F}}_{a,k}(\mathbf{G})|_b - \sum_{k=1}^N \tilde{\mathbf{F}}_{g,k}(\mathbf{G})|_b \quad (33)$$

where  $\mathbf{B}_{j,k} = \begin{pmatrix} \mathbf{0}_{3 \times 3} & \mathbf{0}_{3 \times 3} \\ \mathbf{0}_{3 \times 3} & \mathbf{b}_{j,k} \end{pmatrix}$  is the gyroscopic damping matrix.

Furthermore, the aerodynamic force is linearized such as:

$$\tilde{\mathbf{F}}_{a,k}(\mathbf{G})|_b = \tilde{\mathbf{F}}_{a,k,0}(\mathbf{G})|_b - \mathbf{B}_{a,k}(\omega_e)\dot{\mathbf{X}} \quad (34)$$

where  $\mathbf{B}_a$  is the aerodynamic damping matrix derived from (9) using numerical differentiation.

Taking into account the small amplitude motions assumption, the effect of gravity can be written:

$$\tilde{\mathbf{F}}_{g,k}(\mathbf{G})|_b = \tilde{\mathbf{F}}_{g,k,0}(\mathbf{G})|_b - \mathbf{K}_{g,k}\mathbf{X} \quad (35)$$

with:

•

$$\tilde{\mathbf{F}}_{g,k,0} = -m_k g \begin{pmatrix} 0 \\ 0 \\ 1 \\ \xi_{r,k} \\ -\chi_{r,k} \\ 0 \end{pmatrix} \quad (36)$$

•

$$\mathbf{K}_{g,k} = m_k g \begin{pmatrix} 0 & 0 & 0 & 0 & -1 & 0 \\ 0 & 0 & 0 & 1 & 0 & 0 \\ 0 & 0 & 0 & 0 & 0 & 0 \\ 0 & 0 & 0 & -(\zeta_{r,K} + h) & 0 & 0 \\ 0 & 0 & 0 & 0 & -(\zeta_{r,k} + h) & 0 \\ 0 & 0 & 0 & \xi_{r,k} & \chi_{r,k} & 0 \end{pmatrix} \quad (37)$$

Eventually, the equation of motion of the ship equipped with  $N$  rotors can be re-written:

$$\begin{aligned}
& [\mathbf{M} + \mathbf{A}(\omega_e) + \sum_{k=1}^N \delta \mathbf{m}_{r,k}] \ddot{\mathbf{X}} + (\mathbf{B}(\omega_e) + \mathbf{B}_{\text{ITTC}}(\omega_e) + \sum_{k=1}^N \mathbf{B}_{a,k}(\omega_e) + \sum_{k=1}^N \mathbf{B}_{j,k}(\omega_e)) \dot{\mathbf{X}} + [\mathbf{K} + \sum_{k=1}^N \mathbf{K}_{g,k}] \mathbf{X} \\
& = A_s(\omega_e) \mathbf{F}_e(\omega_e) + \tilde{\mathbf{R}}_{w,0}(\mathbf{G})|_b - \sum_{k=1}^N \tilde{\mathbf{F}}_{a,k,0}(\mathbf{G})|_b + \tilde{\mathbf{F}}_b(\mathbf{G})|_b + \sum_{k=1}^N \tilde{\mathbf{F}}_{g,k,0}
\end{aligned} \tag{38}$$

Moreover, it is assumed that:

- The ship forward speed  $U$ , drift velocity  $U_{\perp}$  and average heading are constant. Therefore,  $\tilde{\mathbf{R}}_{w,0}(\mathbf{G})|_b - \sum_{k=1}^N \tilde{\mathbf{F}}_{a,k,0}(\mathbf{G})|_b$  must be equal to 0.
- The location of the rotors on the ship's deck respects the fore-aft and port-starboard symmetries. Therefore,  $\sum_{k=1}^N \chi_{r,k} = \sum_{k=1}^N \xi_{r,k} = 0$ .

This finally leads to:

$$[\mathbf{M} + \mathbf{A}(\omega_e) + \sum_{k=1}^N \delta \mathbf{m}_{r,k}] \ddot{\mathbf{X}} + (\mathbf{B}(\omega_e) + \mathbf{B}_{\text{ITTC}}(\omega_e) + \mathbf{B}_a(\omega_e) + \sum_{k=1}^N \mathbf{B}_{j,k}(\omega_e)) \dot{\mathbf{X}} + (\mathbf{K} + \mathbf{K}_g) \mathbf{X} = A_s(\omega_e) \mathbf{F}_e(\omega_e) \tag{39}$$

with:

$$\mathbf{K}_g = \begin{pmatrix} 0 & 0 & 0 & 0 & 0 & 0 \\ 0 & 0 & 0 & 0 & 0 & 0 \\ 0 & 0 & 0 & 0 & 0 & 0 \\ 0 & 0 & 0 & -\sum_{k=1}^N m_k g (\zeta_{r,K} + h) & 0 & 0 \\ 0 & 0 & 0 & 0 & -\sum_{k=1}^N m_k g (\zeta_{r,k} + h) & 0 \\ 0 & 0 & 0 & 0 & 0 & 0 \end{pmatrix} \tag{40}$$

As one can expect, the coefficients of the matrix  $\mathbf{K}_g$  are negative corresponding to the well-known destabilizing effect of adding masses above a ship gravity center.

In this study, the BEM software NEMOH has been used (Babartit and Delhommeau, 2015) to calculate the hydrodynamic coefficients ( $\mathbf{A}(\omega_e)$ ,  $\mathbf{B}(\omega_e)$ ,  $\mathbf{F}(\omega_e)$ ). Note that NEMOH does not take into account the forward velocity. Therefore, no corrections have been applied on the hydrodynamic coefficients. The hull mesh used for the hydrodynamic calculations (see Figure 6) was generated using the NEMOH's mesh generator. The mesh is composed of 560 panels which was found to be enough to achieve convergence.

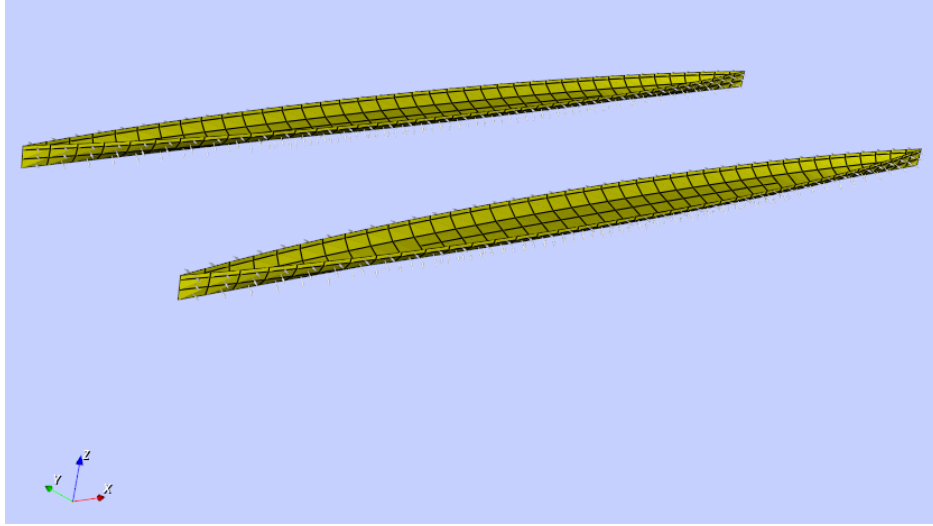


**Figure 6. Hull mesh of the example energy ship design**

The damping matrix correction  $\mathbf{B}_{ITTC}$  is computed as follows :

$$\mathbf{B}_{ITTC} = \mathbf{B}_L + \int_{x_0=-L_{PP}/2}^{L_{PP}/2} (\mathbf{B}'_F + \mathbf{B}'_E) dx_0 + \int_{l=0}^{L_{SK}} \mathbf{B}'_{SK0} dl \quad (41)$$

Where  $\mathbf{B}_L$ ,  $\mathbf{B}'_F$ ,  $\mathbf{B}'_E$  and  $\mathbf{B}'_{SK0}$  are respectively the hull lift damping matrix, hull friction damping matrix per unit length, hull eddy damping matrix per unit length, and appendage damping matrix per unit length. In this study, the appendages are modelled as skegs.  $L_{SK}$  is the sum of the chord length of the appendages and  $L_{PP}$  is the boat length between its perpendiculars (in this case the waterline length). One can find in Table 2 the necessary data to compute the terms in Equation (41) for the example energy ship design shown in Figure 1.

**Table 2. Data used for the computation of the damping matrix  $B_{ITTC}$  (see ITTC (2011) for details)**

Hull related terms	Unit	Value	Appendage related terms	Unit	Value
$A_{HL}$	m <sup>2</sup>	336	$l$	m	17.5
$V$	m/s	9.00	$L_{SK}$	m	6.00
$L_{PP}$	m	80.0	$b_{SK}$	m	0.200
$d$	m	2.10	$l_{sk}$	m	8.00
$l'_0$	m	14.9	$l_1$	m	13.5
$l'_r$	m	15.2	$l_2$	m	1.54
$OG$	m	14.6	$l_3$	m	0
$b_{demi}$	m	12.6	$a$	m <sup>2</sup>	3.44

### 3 RESULTS

The models were implemented in Python. The integrals in the rotor model were replaced by finite sums. The rotors were discretized in 25 elements which were found to be enough in practice to achieve convergence. In this study, we assumed  $U = 9$  m/s,  $W_{10} = 9$  m/s and  $SR = 3.5$  corresponding to the nominal conditions for the energy ship design of Ecole Centrale de Nantes (Babarit et al., 2021).

#### 3.1 Validity of the linear damping model

In order to investigate whether the linear damping model gives an acceptable approximation of the aerodynamic force, let us consider a single rotor in roll motion.

Figure 7 shows the aerodynamic moment variation  $\Delta M_{a,x}(B)$  as a function of the roll motion  $\varphi(t) = A_\varphi \sin(\omega t)$  and the roll velocity  $\dot{\varphi}(t) = A_\varphi \omega \cos(\omega t)$  computed using the quasi-static approach (Equation 8) and its linearization (Equation 14). The roll motion amplitude  $A_\varphi$  was set to  $5^\circ$  and  $15^\circ$ . Two periods  $T = \frac{2\pi}{\omega}$  were considered : 5 s and 10 s. The combination of  $A_\varphi = 15^\circ$  and  $T = 5$  s is not considered for sake of brevity. For better understanding, the motion and velocities were expressed in degrees and degrees per seconds respectively in the first column.

Figure 7 shows that there are significant differences between the linear model and the quasi-static model. Even for the smallest motion amplitude and the longest period, the linear model overestimates the variation in aerodynamic moment by 26 %. Therefore, the linear model appears to be only a coarse approximation of the effect of motion on the aerodynamic force.

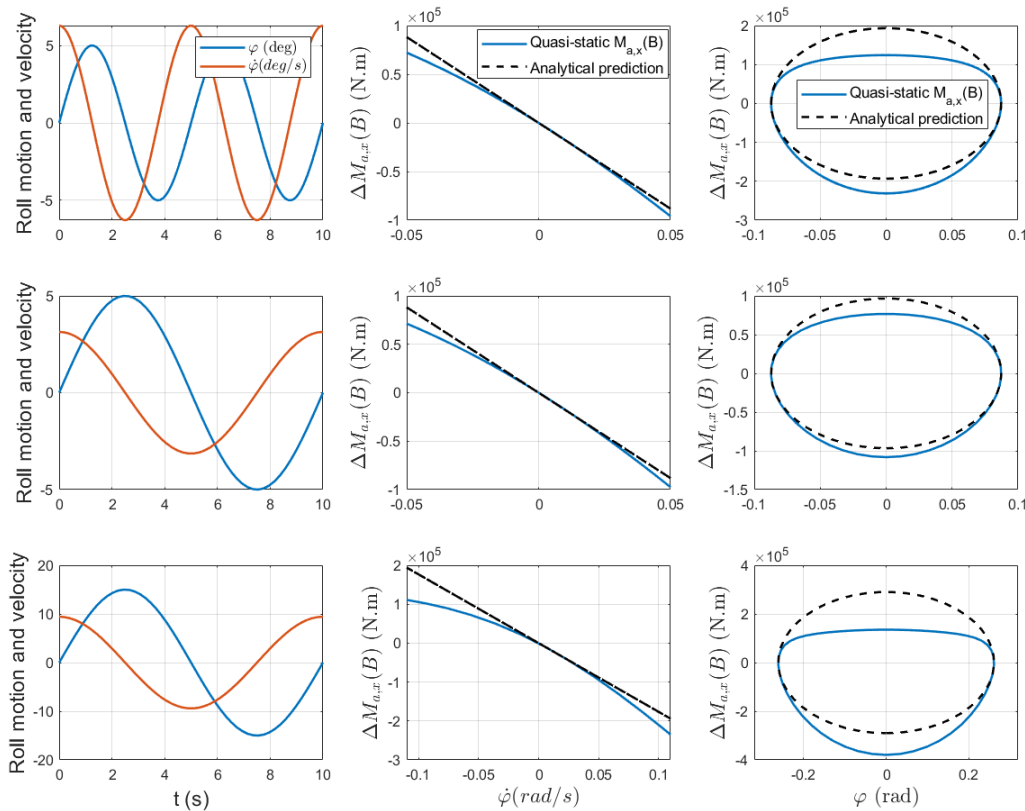


**Figure 7.** From left to right, forced roll angle and velocity, aerodynamic moment  $\Delta M_{a,x}(B)$  and its linearization. First row for  $T = 5$  s and  $A_\varphi = 5^\circ$ , second row for  $T = 10$  s and  $A_\varphi = 5^\circ$ , third row for  $T = 10$  s and  $A_\varphi = 15^\circ$ . Computed for  $U = 9$  m/s,  $SR = 3.5$  and  $W_{10} = 9$  m/s

### 3.2 Aerodynamic damping effect in regular waves

The response amplitude operators (RAOs) of the proposed energy ship in beam waves were calculated according to Equation 30 and the linearized aerodynamic damping model (Equation 15). The gyroscopic damping matrix is not considered in this section. The wave amplitude is 0.50 m for all wave frequencies. Note that aerodynamic interactions between the four rotors were neglected in this study.

Results are shown in Figure 8. The continuous blue curve corresponds to the predicted ship response with only wave radiation damping (aerodynamic damping and ITTC correction are neglected). The dashed red curve shows the response with both aerodynamic and wave radiation damping. The

continuous red curve with round markers shows the response with both ITTC and wave radiation damping (aerodynamic damping is neglected). The dashed black curve shows the response with all damping sources. Note that the RAOs in surge, pitch and yaw are not shown since the response for these degrees of freedom is small compared to the others (less than  $10^{-3}$  m/m or  $^{\circ}$ /m).

Results show that for this particular ship design and wind/wave conditions, the Flettner rotors are destabilizing in roll. Indeed, taking into account aerodynamic damping increases the maximum roll angle by 6 % in comparison to that with only wave radiation damping (right panel in Figure 8). However, if the damping model including ITTC corrections for hull and appendages in addition to wave radiation damping is considered as a reference, one can see that taking into account aerodynamic damping leads to an increase of the maximum roll angle by 4 %. Therefore, the seakeeping behaviour of the energy ship design shown in Figure 1 appears not to be significantly affected by the aerodynamic damping effect from the Flettner rotors, at least for the considered operating conditions.

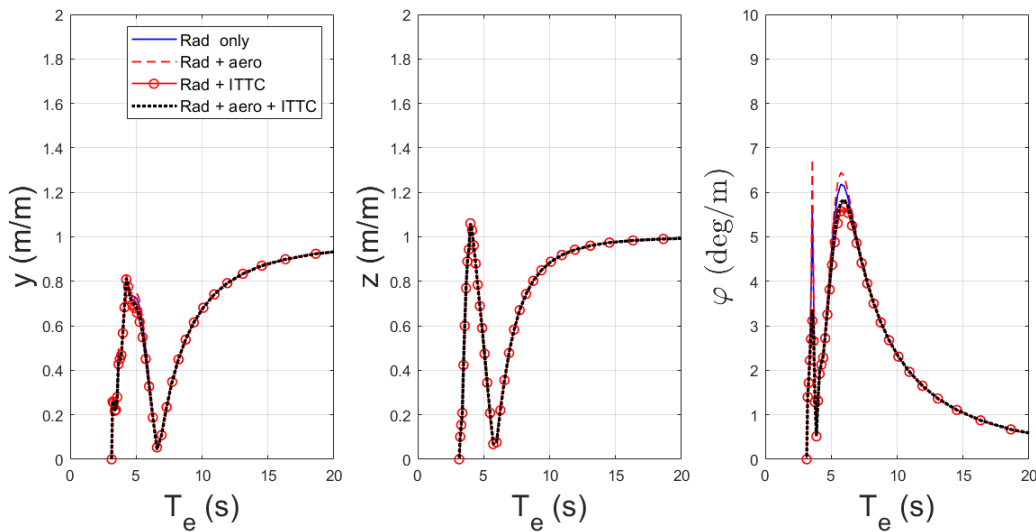


**Figure 8. RAOs of the example energy ship in regular beam waves. The wave amplitude is 0.50 m for all wave frequencies. Other parameters are  $U_s = 9$  m/s,  $\beta=90^{\circ}$ ,  $W_0 = 9$  m/s and  $SR=3.5$**

### 3.3 Gyroscopic effect in regular waves

This section presents the RAOs of the proposed energy ship in beam waves taking into account both aerodynamic damping and gyroscopic damping from the rotors. The mass considered in the calculation of the rotor's moment of inertia (the actual rotating mass) is supposed to be equal to 10 t.

Figure 9 shows the RAO in sway, heave, roll and pitch. The dotted blue curve corresponds to the energy ship with all the damping sources considered in section 3.2 without the gyroscopic effects while the continuous black curve represents an energy ship with all the considered damping sources and the gyroscopic damping from the rotors.

One can see that the gyroscopic effect is negligible for sway, heave and roll. For pitch, there appears to be a small destabilizing effect, which is expected because from Equation 27 we know that a coupling exists between the pitch motion and the forced pure roll motion. Nevertheless, the resulting maximum pitch motion is very small (less than  $0.06^{\circ}$ /m which approximately corresponds to an aft/forward draft of 4 cm for  $A_s = 0.5m$ ).

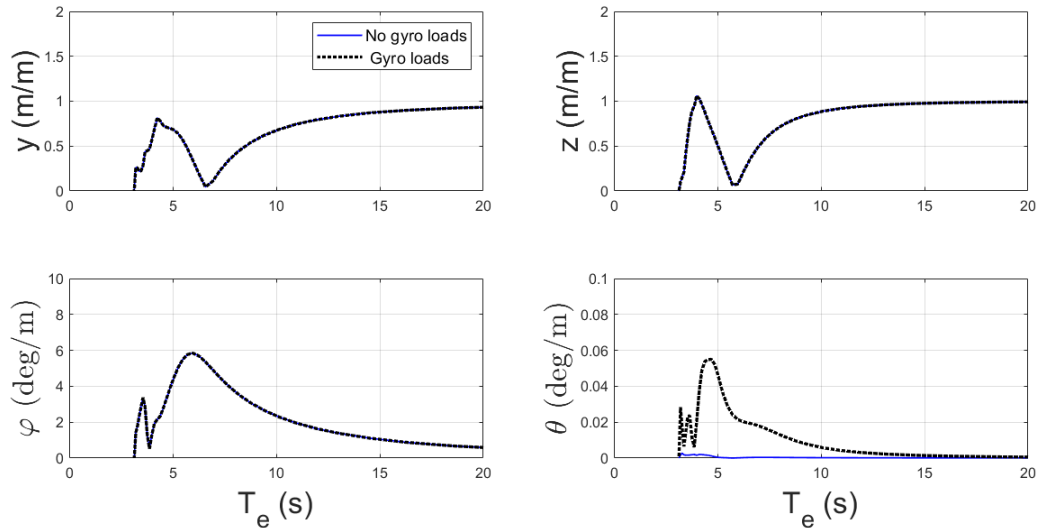


**Figure 9. Rotor gyroscopic effect on ship motions for the example energy ship in regular beam waves. The wave amplitude is 0.50 m for all wave frequencies. Other parameters are  $U_s = 9$  m/s,  $\beta=90^\circ$ ,  $W_0 = 9$  m/s and  $SR=3.5$**

### 3.4 Effect of increased rotor mass

In this section, we investigate the effect of the rotor mass on the motion response. According to Equation 40, the effect of increasing the rotor mass is destabilizing as it reduces the total stiffness matrix.

The seakeeping calculations were performed using the same loads as described in section 3.2 except that the gyroscopic effects are not considered. Figure 10 shows the RAOs of the example energy ship for sway, heave and roll for the reference rotors' mass, a rotors' mass increased by 10 % and a rotors' mass reduced by 10%. Results show that for this range of variations of the rotors' mass, the effect on the ship response is too small to be visible.

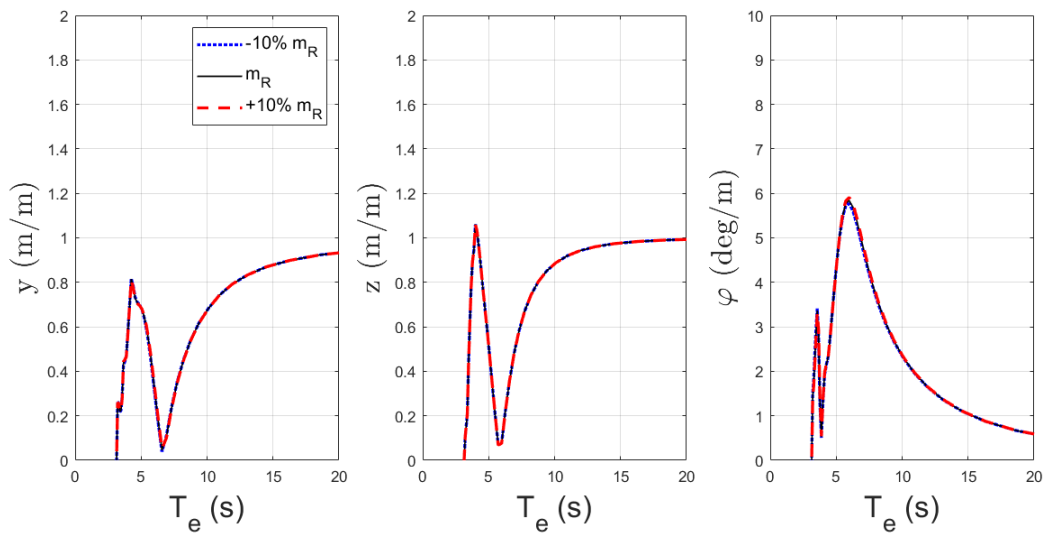


**Figure 10. Effect of variations of the rotors' mass on the ship response to regular beam waves. The wave amplitude is 0.50 m for all wave frequencies. Other parameters are  $U_s = 9$  m/s,  $\beta=90^\circ$ ,  $W_0 = 9$  m/s and  $SR=3.5$**

## 4 CONCLUSIONS

In this study, we investigated the effect of Flettner rotors on the seakeeping of an energy ship. The considered effects are aerodynamic damping, gyroscopic effect and the effect of increasing and decreasing rotors' mass.

For the aerodynamic damping, the rotors were modelled using a quasi-static approach and a linearized approach in order to analyze the effect of the rotor in pure roll motion in beam seas. For a true wind speed and ship velocity of  $W_{10} = 9$  m/s and  $U = 9$  m/s respectively, it is shown that it can be stabilizing if  $SR \in [0, \simeq 0.5] \cup [\simeq 1.5, \simeq 3.1]$ . If  $SR \in [\simeq 0.5, \simeq 1.5]$  or if  $SR > 3.1$ , the rotors are destabilizing. The model was applied to take into account the effect of the rotors in seakeeping calculations. It is found that, for the case study in beam waves for  $SR = 3.5$ , the Flettner rotors have a small destabilizing effect in roll (no effect observed on the other degrees of freedom).

As for the gyroscopic effect of the rotors, it is found that, for the case study in beam waves for  $SR = 3.5$ , it induces a small destabilizing effect in pitch. For the other degrees of freedom, the effect is too small to be visible.

The model was also used to investigate the effect of the rotors' mass on the seakeeping behaviour of the energy ship. Results show that the effect of variations of  $\pm 10\%$  of the rotors' mass is negligible on the ship response.

These results indicate that the most significant effect of Flettner rotors on the seakeeping of an energy ship is aerodynamic damping. Further research is needed on this topic as comparisons between the linear model and the quasi-static model show that the accuracy of the linear model is rather limited even for small amplitude motion. Moreover, the model is based on several simplifications which may affect the conclusions. The strip-wise model of the rotor relies on 2D lift and drag coefficients which were calibrated based on experimental data for a particular rotor (Reynolds number, aspect ratio) on a particular ship (rotor-ship interactions). In the present study, even if the rotor geometry and operational regime are similar to those of the experiments, the rotor-ship interactions may be significantly different because of different ship geometries. Therefore, the 2D coefficients may actually be different for the ship considered in this study compared to that of the experimental data. Another likely highly significant simplification is that the aerodynamic interactions between the rotors were neglected.

Moreover, the model is based on a quasi-static approach. Possible missing dynamic effects are dynamic stall and added mass. It is believed that this assumption is acceptable because the low density of the air compared to that of water makes the aerodynamic added mass negligible compared to the hydrodynamic added mass. Nevertheless, this will have to be verified in future work.

Finally, the seakeeping model used in the present study does not take into account the variation of the hull wetted surface. Indeed, when a catamaran experiences large roll motions, the hydrostatic stiffness matrix changes significantly (especially in the case of hull emergence) thus affecting significantly the prediction of his response to regular beam seas.

## 5 ACKNOWLEDGEMENTS

This work was supported by ANRT (French National Association for Research and Technology).

## REFERENCES

Babarit, A. et al. (2021). "Exploitation of the far-offshore wind energy resource by fleets of energy ships – Part 2: Updated ship design and cost of energy estimate." In: *Wind Energy Science* 6.5, pp. 1191–1204.

- Babarit, Aurélien and Gérard Delhommeau (2015). "Theoretical and numerical aspects of the open source BEM solver NEMOH". In: *Proc. of the 11th European Wave and Tidal Energy Conference (EWTEC2015)*. Nantes, France.
- Clayton, B.R. (1985). "BWEA initiative on wind assisted ship propulsion". In: *Proc. of the International Symposium on Windship Technology (WINDTECH '85)*. Southampton, U.K.: ASME.
- Copuroglu, Hasan Islam and Emre Pesman (2018). "Analysis of Flettner Rotor ships in beam waves". In: *Ocean Engineering* 150, pp. 352–362.
- Demir, Uğursal (Dec. 2020). "Use of Anti Rolling Gyro (ARG) Optimization Systems For Planing Boats". In: 2, pp. 247–261. DOI: 10.47898/ijeased.794333.
- F.M.Sinclair (1991). "The motion damping characteristics of wind energy devices". PhD thesis. University College London.
- Faltinsen, O (1993). *Sea Loads on Ships and Offshore Structures*. Cambridge: Cambridge University Press.
- Gilloteaux, Jean-Christophe and Aurelien Babarit (2017). "Preliminary design of a wind driven vessel dedicated to hydrogen production". In: *Proc. of the International Conference on Ocean, Offshore Mechanics and Artic Engineering*. Trondheim, Norway: ASME.
- Ikeda, Yoshiho (1978). "Components of roll damping of ship at forward speed". jap. In: ed. by Department of Naval Architecture University of Osaka Prefecture. Berlin-Boston: Journal of Society of Naval Architects of Japan, pp. 21–54.
- IPCC et al. (Dec. 2018). *Global warming of 1.5°C. An IPCC Special Report on the impacts of global warming of 1.5°C above pre-industrial levels and related global greenhouse gas emission pathways, in the context of strengthening the global response to the threat of climate change, sustainable development, and efforts to eradicate poverty*.
- ITTC (2011). "Numerical estimation of roll damping." In: *ITTC-Recommended procedures*. Gosport, UK: 6th ITTC Specialist Committee on Stability in Waves, pp. 7.5-02-07–04.5.
- Katayama, Toru, Masanori Kotaki, and Yoshiho Ikeda (2011). "A Study on the Characteristics of Roll Damping of Multi-Hull Vessels". In: vol. 97, pp. 487–498.
- Kim, J. and C. Park (2010). "Wind power generation with a parawing on ships, a proposal". In: *Energy* 35, pp. 1425–1432.
- Kuuskoski, J. and Paakkari V. (2023). "Building trust in thrust". In: *Proc. of the Wind Propulsion conference*. London, UK: The Royal Institution of Naval Architects, pp. 25–31.
- Li, D. and B. Leer-Andersen M. Allenström (2012). "Performance and vortex formation of Flettner rotors at high Reynolds numbers". In: *29th international Symposium on Naval Hydrodynamics*. Gotenburg.
- Ouchi, K. and J. Henzie (2017). "Hydrogen generation sailing ship: conceptual design and feasibility study". In: *In Proc. of the OCEANS conference*. Institute of Electrical and Electronics Engineers.
- Perez, Tristan and Paul D. Steinmann (2009). "Analysis of Ship Roll Gyrostabiliser Control". In: *IFAC Proceedings Volumes* 42.18. 8th IFAC Conference on Manoeuvring and Control of Marine Craft, pp. 310–315. ISSN: 1474-6670. DOI: <https://doi.org/10.3182/20090916-3-BR-3001.0007>. URL: <https://www.sciencedirect.com/science/article/pii/S1474667016319139>.

Platzer, Maximilian et al. (2014). "Renewable energy production using sailing ships". In: *ASME Journal of Energy Resources Technology* 136.

Salomon, R.E. (1982). *Process of converting wind energy to elemental hydrogen and apparatus therefore*. U.S. Patent 4335093A.

Tillig, Fabian and Jonas W. Ringsberg (2020). "Design, operation and analysis of wind-assisted cargo ships." In: *Ocean Engineering* 211.Number, p. 107603.

Touma, Jawad S. (1977). "Dependence of the Wind Profile Power Law on Stability for Various Locations". In: *Journal of the Air Pollution Control Association* 27, pp. 863–866.